DNA conformations in mismatch repair probed in solution by X-ray scattering from gold nanocrystals

Greg L. Hura[a], Chi-Lin Tsai[a], Shelley A. Claridge[b,1], Marc L. Mendillo[c,2], Jessica M. Smith[a,b], Gareth J. Williams[a], Alexander J. Mastroianni[b,3], A. Paul Alivisatos[a,b], Christopher D. Putnam[c,d], Richard D. Kolodner[c,e,f,g], and John A. Tainer[a,h,4]

[a]Lawrence Berkeley National Laboratory, Berkeley, CA 94720; [b]Department of Chemistry, University of California, Berkeley, CA 94720; [c]Ludwig Institute for Cancer Research, La Jolla, CA 92093; Departments of [d]Medicine and [e]Cellular and Molecular Medicine, [f]Cancer Center, and [g]Institute of Genomic Medicine, School of Medicine, University of California, San Diego, La Jolla, CA 92093; and [h]The Skaggs Institute for Chemical Biology, The Scripps Research Institute, La Jolla, CA 92037

Edited by James M. Berger, The Johns Hopkins University School of Medicine, Baltimore, MD, and approved September 11, 2013 (received for review May 6, 2013)

DNA metabolism and processing frequently require transient or metastable DNA conformations that are biologically important but challenging to characterize. We use gold nanocrystal labels combined with small angle X-ray scattering to develop, test, and apply a method to follow DNA conformations acting in the *Escherichia coli* mismatch repair (MMR) system in solution. We developed a neutral PEG linker that allowed gold-labeled DNAs to be flash-cooled and stored without degradation in sample quality. The 1,000-fold increased gold nanocrystal scattering vs. DNA enabled investigations at much lower concentrations than otherwise possible to avoid concentration-dependent tetramerization of the MMR initiation enzyme MutS. We analyzed the correlation scattering functions for the nanocrystals to provide higher resolution interparticle distributions not convoluted by the intraparticle distribution. We determined that mispair-containing DNAs were bent more by MutS than complementary sequence DNA (csDNA), did not promote tetramer formation, and allowed MutS conversion to a sliding clamp conformation that eliminated the DNA bends. Addition of second protein responder MutL did not stabilize the MutS-bent forms of DNA. Thus, DNA distortion is only involved at the earliest mispair recognition steps of MMR: MutL does not trap bent DNA conformations, suggesting migrating MutL or MutS/MutL complexes as a conserved feature of MMR. The results promote a mechanism of mismatch DNA bending followed by straightening in initial MutS and MutL responses in MMR. We demonstrate that small angle X-ray scattering with gold labels is an enabling method to examine protein-induced DNA distortions key to the DNA repair, replication, transcription, and packaging.

DNA is frequently considered a passive component in interactions with proteins involved in DNA metabolism. Despite this view, many proteins use DNA structural features to mediate catalysis and identify damaged DNA through the effects of damage on DNA rigidity and conformation (1–6). The view of DNA as a passive element is therefore at least in part due to a paucity of robust tools to examine dynamic DNA conformational states during multistep reactions. Gold-labeled DNA enables measurement over length scales sufficient to accommodate several proteins to identify cooperative effects on DNA. Because X-rays scatter predominantly from electrons, using heavy atom labels (7–11) provides high contrast relative to organic molecules. By using labels of moderate size (~5 nm), the scattering from gold nanocrystals dominates all other scattering signals by three orders of magnitude, thereby reducing analysis complexity while minimizing nanocrystal influence on biological macromolecules. Importantly, small angle X-ray scattering (SAXS) provides global information on conformations adopted by a population of macromolecules in almost any solution condition (12–14).

Mismatch repair (MMR) is an evolutionarily conserved process that corrects mismatches generated during DNA replication (15, 16). Despite the importance of MMR in recognition and excision of mispairs introduced by replication errors or chemical damage to avoid genome instability and cancer (17), key mechanistic steps remain incompletely understood. In both prokaryotes and eukaryotes, MMR begins when the enzyme MutS or a MutS homolog dimer recognizes mispairs in a nucleotide-free or ADP-bound state. In *Escherichia coli*, the protein MutL is then recruited to activate downstream steps leading to the excision of the mismatched base and surrounding bases and resynthesis of the strand to complete repair (15). The crystal structures of MutS and homologs bound to mispaired DNA substrate bent the DNA by ~60° from linear at the mispair (2, 4, 18). Mispair-dependent exchange for ATP, which allows conversion of MutS into a sliding clamp form and binding to a MutL dimer, is required for downstream MMR processes (19–22). Although structural aspects of latter states have been inferred by indirect probing of MutS (21, 23–25), decades of research have led to multiple hypotheses regarding the function of DNA bending and the importance of MutS sliding. These DNA states that are thought to be crucial to MMR in vivo have proven resistant to analysis at atomic resolution (26). Consequently, the role of DNA conformations in damage signaling and repair protein recruitment has remained enigmatic (15).

Significance

We developed and applied nanogold labels for DNA complexes with proteins examined by small angle X-ray scattering (SAXS) to follow DNA conformations acting in error detection by the mismatch repair (MMR) system in solution. This technique can examine short or long pieces of DNA and in most solution conditions, including those closest to cellular environments. Thus, we expect the technique to be useful for many biologically important systems involving DNA complexes and conformations. Specifically, we reveal DNA bending followed by straightening by the repair protein MutS at the site of a mismatch as a suitable mechanism for error detection and signaling needed to avoid mutations and cancers and to control microbial stability and evolution in response to environmental stress.

Author contributions: G.L.H., G.J.W., C.D.P., R.D.K., and J.A.T. designed research; G.L.H., C.-L.T., S.A.C., M.L.M., J.M.S., G.J.W., A.J.M., A.P.A., C.D.P., R.D.K., and J.A.T. performed research; G.L.H., C.-L.T., S.A.C., M.L.M., J.M.S., G.J.W., A.P.A., C.D.P., R.D.K., and J.A.T. contributed new reagents/analytic tools; C.D.P., R.D.K., and J.A.T. analyzed data; and G.L.H., C.D.P., R.D.K., and J.A.T. wrote the paper.

The authors declare no conflict of interest.

This article is a PNAS Direct Submission.

Freely available online through the PNAS open access option.

[1]Present address: California Nanosystems Institute and Department of Chemistry and Biochemistry, University of California, Los Angeles, CA 90095.

[2]Present address: Whitehead Institute for Biomedical Research, Cambridge, MA 02142.

[3]Present address: Life Technologies, Foster City, CA 94404.

[4]To whom correspondence should be addressed. E-mail: jat@scripps.edu.

This article contains supporting information online at www.pnas.org/lookup/suppl/doi:10.1073/pnas.1308595110/-/DCSupplemental.

To characterize DNA conformational changes acting in MMR quantitatively, we herein build upon previous SAXS studies of naked DNA with gold nanocrystal labels (9–11). Our results show MutS bending of mispair-containing DNAs is greater than for complimentary sequence DNA (csDNA), that the ATP-mediated conversion of MutS to a sliding clamp involves loss of the DNA bend, and that MutL does not function to stabilize a MutS-mediated bend, in contrast to some MMR models. SAXS with gold labels has accurately measured properties of DNA (9–11). As used here, SAXS with gold labels is a promising method for the study of DNA processing by cooperative enzymes where solution conditions, long distances, low concentrations, substoichiometric populations, and short time scales are of importance.

Results

High Scattering Power and Dominant Signal of Gold Nanocrystals. To examine DNA conformations in solution by SAXS, we selected gold nanocrystal labels with a nominal diameter of 5 nm. Gold atoms are electron-rich and densely packed in the nanocrystal (19.3 g/cm^3), and thus have an electron density over 10-fold that of protein (4.6e-/Å^3 for gold nanocrystals vs. 0.43 and 0.55e-/Å^3 for protein or DNA, respectively). Because the scattering power is weighted by the square of the difference in electron density, $\Delta\rho$, between solvent and particle, adjusting the average electron density of the solvent to match the density of protein can further magnify the relative increase in scattering by the gold nanocrystal. In water, the measured scattering of a gold nanocrystal with a 5-nm diameter was 200-fold higher than that of a 172-kDa protein and 5,400-fold higher than that of 31-bp dsDNA (*SI Appendix*, Fig. S1). Thus, measured scattering in mixed systems containing gold nanocrystals, nucleic acids, and proteins is dominated by the gold signal, whereas protein, DNA, and DNA/gold scattering cross-terms are insignificant.

Synthesis of Gold-Labeled DNA for Reproducible and Accurate Distance Determinations. The challenge of using commercially available gold nanocrystals for synthesizing gold-labeled DNA was to ensure compatibility of the nanomaterials with the biological macromolecules. Several gold nanocrystal ligands were investigated for compatibility with DNA and the *Escherichia coli* MutS. An anionic carboxy-terminated PEG ligand for the nanocrystal labels proved problematic because the measured distance between two nanocrystal labels placed on both ends of the dsDNA molecule decreased 15% with increasing NaCl concentration (*SI Appendix*, Fig. S2). We found, however, that gold nanocrystals coated with a neutral PEG ligand provided invariant distances when conjugated to both ends of dsDNA within the salt concentrations tested (0–200 mM NaCl) and did not precipitate MutS; thus, this ligand was used in the bulk of our studies.

Determination of the Correlation Scattering Factor and Analysis of the X-Ray Scattering from Labeled DNA. As in previous studies (9–11), we collected scattering data from isolated labels and from labeled dsDNA molecules (Fig. 1). Gold nanocrystals dominated the scattering, so we could directly analyze the scattering profiles of the labeled DNA using the Debye approximation for systems of equivalent particles as previously reported (11). For two labels, the total scattering $I(q)$ is the sum of scattering from individual labels $G(q)$ and a correlation term, which is a Fourier transform of the distribution of distances between labels, $P(D_{i,j})$ (27):

$$I(q) = 2G(q) + 2G(q)\sum_{i,j}^{N} P(D_{i,j})\sin(qD_{i,j})/(qD_{i,j}).$$

The correlation scattering factor (CSF), which is a Fourier transform of $P(D_{i,j})$, oscillates about zero and can be extracted from the experimental data by rearranging the Debye approximation (9–11):

$$\mathrm{CSF}(q) = I(q)/[kG(q)] - 1.$$

Nominally, the value of the parameter k is 2; however, the parameter was influenced by experimental factors, such as the amount of unconjugated labels due to contamination or radiation-induced cleavage. Thus, the parameter was fitted during the CSF calculation (*SI Appendix*, Fig. S3).

To calculate the CSF, we determined the scattering term from individual labels, $G(q)$, by fitting the scattering of a solution of nonconjugated gold nanocrystals because we found that noise in the experimental scattering from labels introduced artifacts in the CSF. Homogeneous spheroid models of the gold nanocrystals fit the SAXS profile poorly; the nanocrystal labels have a size distribution and unequal axis lengths as revealed by transmission EM (TEM) (*SI Appendix*, Fig. S4). Fitting the scattering using homogeneous ellipsoids of rotation had excellent agreement to the unconjugated label with a χ^2 value of 1 for the scattering over the critical region of $q < 0.1$ Å^{-1}, and thus did not require generation of distributions of atomic models for this purpose (Fig. 1). Batch-to-batch variation in the size of gold nanocrystals was observed. For example, nanocrystals used to label the 31-bp dsDNA were best fit by an ellipsoid of rotation with semiaxis dimensions of 28 × 28 × 41 Å, and nanocrystals used to label the 71-bp dsDNA were best fit by an ellipsoid with semiaxis dimensions of 27 × 27 × 38 Å (*SI Appendix*, Fig. S1*B*). Examination of TEM images for labels yielded mean largest and smallest semiaxis dimensions of 32 with an SD of 4 Å and 29 with an SD of 4 Å, respectively. Agreement between SAXS and TEM is within the expected limits, because ellipsoidal particles will not uniformly present themselves with their longest axis perpendicular to view, making them appear more spherical. As expected, the CSF functions calculated for unconjugated labels and dsDNA molecules with a single label had a featureless CSF because the scattering was dominated by the form factor of a single gold label. In contrast, the CSF functions from dsDNA molecules with two labels had a decaying oscillatory behavior (Fig. 1).

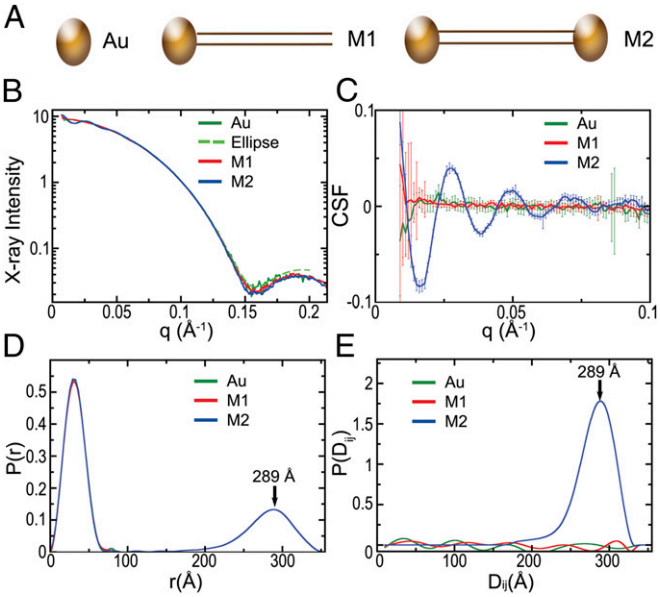

Fig. 1. Sensitive SAXS measurements on DNA: Analysis of a gold nanocrystal (Au), end-labeled 71-bp DNA with a single gold nanocrystal (M1), and doubly end-labeled 71-bp DNA (M2). (*A*) Diagram of samples analyzed. (*B*) Scattered X-ray intensity from Au, M1, M2, and the fit of Au to an ellipsoid ($a = b = 26.8$ Å, $c = 38$ Å). (*C*) CSF was derived from the scattered intensity and the fitted ellipsoid. (*D*) *P(r)* function was calculated from *I*(*q*) by the GIFT. (*E*) $P(D_{i,j})$ function was calculated from the CSF by the GIFT.

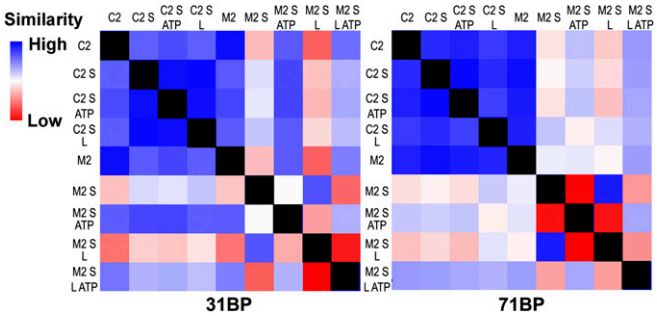

Fig. 2. SAXS similarity maps from 31- and 71-bp DNA. SAXS profiles from doubly labeled DNA substrates with a mismatch (M2) and complementary (C2) in the presence of MutS (S), MutL (L), ATP, and combinations are scored for pair-wise agreement and assigned a gradient color (12) ranging from high similarity (blue) to low similarity (red).

The distributions of distances between the centers of mass of the gold nanocrystal labels, $P(D_{i,j})$, were derived from the CSF by the generalized indirect Fourier transform (GIFT) method (28). In contrast to the pair-distribution function, $P(r)$, which is generated by applying the GIFT to $I(q)$, the $P(D_{i,j})$ derived from the CSF lacks intraparticle information, and hence is robust to small amounts of unconjugated gold labels (Fig. 1). The maximum values of the $P(D_{i,j})$ distribution on the doubly labeled 31-, 50-, 61-, 71-, and 91-bp dsDNAs were 181, 228, 269, 292, and 346 Å, respectively. These give an average increase in length per base pair of 2.8 ± 0.2 Å. The reduced length per base pair relative to the crystallographic average rise per base pair of 3.32 ± 0.19 Å (29) is in agreement with previous time-resolved fluorescence resonance energy transfer, double-electron spin resonance, and SAXS (10, 11). As reported previously (11), the measured shorter distance per base pair subsumes DNA bending and the effective distance is consistent with crystallographic values in a worm-like chain model for DNA calculated with a persistence length of 50 nm and a 3.4-Å rise per base pair. The transformation of the CSF by the GIFT algorithm also effectively quantified samples containing subpopulations with differing gold-to-gold distances in experiments where 31- and 61-bp dsDNAs were mixed in defined ratios (*SI Appendix*, Fig. S5).

The theoretical $P(D_{i,j})$ distribution of a perfectly rigid and homogeneous population is an infinitely sharp peak at a single distance. In practice, the $P(D_{i,j})$ distributions are broadened by the nonsphericity of the gold nanocrystals, the distribution of gold nanocrystal sizes, flexibility of the DNA-label linker, bending of the DNA, and approximations in the GIFT construction of the $P(D_{i,j})$ distribution. For the dsDNA molecules investigated here, we did not observe a trend for increasing width of the peaks at the half-maximum value with increasingly long DNAs, suggesting that the width of the peaks at half-maximum, ranging from 44 to 67 Å, was dominated by factors other than DNA bending.

MutS Bends Mispaired DNA More than Fully csDNA. MutS binds and bends mispair-containing DNA molecules in the absence of ATP (2, 4, 18, 30). MutS, however, only has a 10- to 20-fold discrimination of mispair-containing DNA to fully csDNA (17), and atomic details of interactions of MutS on csDNA are not available, although deuterium exchange and single-molecule experiments have suggested that MutS and the MutS homologs bind csDNA as a weakly bound ring (24, 31–33). We thus probed the effects of MutS binding dsDNA molecules with two gold nanocrystal end labels either with (M2) or without (C2) a central G/T mispair. The available crystal structures of *E. coli* MutS and homologous proteins indicate that ∼20 bp are contacted (2, 4, 18, 30); thus, we investigated substrates that were 31 or 71 bp long. Comprehensive views of SAXS were examined in a structural comparison map (12) derived directly from comparing CSFs (Fig. 2). The small changes induced by MutS on csDNA relative to mismatch are demonstrated by the all blue (similar) C2 quadrant compared with the differences observed in the lower left quadrant for both substrate lengths.

E. coli MutS forms tetramers, with a reported K_d for the dimer/tetramer equilibrium ranging from 210 to 2,200 nM^{-1} (34, 35), that could complicate the analysis of the $P(D_{i,j})$ distributions if mixed populations of dimers and tetramers were present. Use of the gold nanocrystals, however, allowed us to make measurements at protein concentrations as low as 50 nM, well below the K_d. To test if tetramers were present during mismatch DNA recognition under our conditions, we bound MutS to 71-bp dsDNAs conjugated to a single gold label with (M1) or without (C1) a central G/T mispair: We did not observe a signal in the CSF or a peak in the $P(D_{i,j})$ distribution (*SI Appendix*, Fig. S6). Moreover, we repeated the experiments with doubly labeled substrates with the MutSΔ800 mutant protein, which lacks the C-terminal domain required for tetramerization, and the MutS-R840E mutant protein, which disrupts tetramerization (36, 37). The CSFs from the modified protein were identical to within noise for each condition. These results show that tetramers of MutS simultaneously bound to two DNA molecules were not present at significant concentrations, suggesting tetramer formation is not a response to binding mismatch DNA.

MutS had little or no effect on the scattering of the 31- and 71-bp C2 substrates, which lacked a central mispair (Fig. 3 *A* and *C*), whereas it strongly affected the scattering of the 31- and

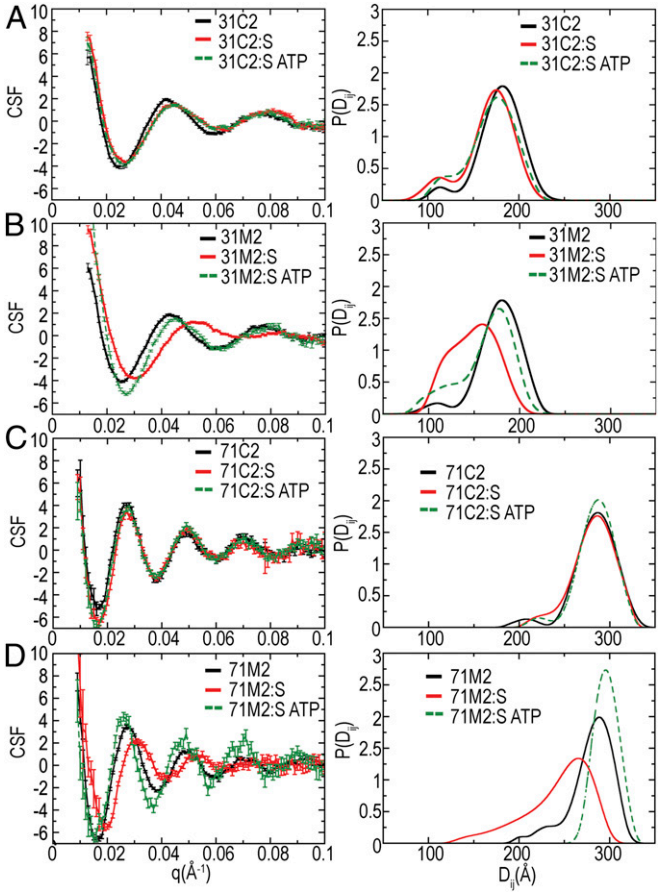

Fig. 3. MutS bends mispaired DNA much more than csDNA, as shown by the CSF and $P(D_{i,j})$ distributions from doubly labeled DNA in the presence of MutS and ATP. (*A*) Fully complementary, doubly labeled 31-bp DNA. (*B*) Doubly labeled 31-bp DNA with a single centrally located G/T mismatch. (*C*) Fully complementary, doubly labeled 71-bp DNA. (*D*) Doubly labeled 71-bp DNA with a single centrally located G/T mismatch. All DNA substrates were collected alone (black) in the presence of MutS (red) or MutS and ATP (green dashes).

71-bp M2 substrates, which had a central G/T mismatch (Fig. 3 *B* and *D*). For the 31-bp C2 substrate, MutS binding decreased the position of the $P(D_{i,j})$ peak by 7 Å (Fig. 3*A* and Table 1), which corresponds to the DNA being bent by 32° from linear, assuming that the bend was centrally located. A shift was not observed for the 71-bp C2 substrate (Fig. 3*C* and Table 1), although DNA binding was confirmed by EMSA (*SI Appendix*, Fig. S7). In contrast, MutS strongly affected the scattering of both doubly labeled dsDNAs containing a central G/T mismatch (Fig. 3 *B* and *D*). Addition of 600, 1,200, or 2,400 nM MutS to a 30-nM solution of the 31-bp M2 substrate produced indistinguishable CSFs (*SI Appendix*, Fig. S8). The maximum of the MutS-bound 31-bp M2 $P(D_{i,j})$ distribution shifted from 181 to 159 Å (Fig. 3*B* and Table 1), corresponding to a centrally located bend of 58° from linear, supporting and extending data from crystal structures by solution measurements (2, 4, 18, 30). The peak had an asymmetrical distribution, which suggests multiple static bend angles or dynamic flexing of MutS-bent DNA, and thus supports and extends single-molecule fluorescence experiments (38). Using the low half-maximum values, the bending was as large as 90°. The 110-Å shoulder in the $P(D_{i,j})$ distribution approximated the contact distance between two gold nanocrystals coated with PEG. We also titrated MutS at concentrations between 42 and 360 nM against a 6-nM solution of the 71-bp M2 substrate (*SI Appendix*, Fig. S8). Changes in the $P(D_{i,j})$ distribution appeared to saturate at 180 nM of MutS. The peak of the MutS-bound 71-bp M2 $P(D_{i,j})$ distribution shifted from 289 to 265 Å with an asymmetrical distance distribution (−62 Å, +24 Å at half-maximum) (Fig. 4*D*). Assuming that changes were solely due to bending at the mispair, the DNA bending was 48° from linear (62° using half-maximum values).

Sliding Clamp Form of MutS Does Not Bend DNA. ATP binding by mispair-bound MutS is thought to trigger the conversion of MutS into a sliding clamp, which rapidly dissociates from free DNA ends but not from ends blocked by protein/DNA complexes (21, 22). Because the gold labels used in SAXS are larger than the protein/DNA complexes used to trap the sliding clamp form of MutS on DNA, we used our substrates to analyze what effect the sliding clamp had on the conformation of substrate DNA. Addition of ATP to the 31-bp or 71-bp C2/MutS complexes had little effect, shifting the peak in the $P(D_{i,j})$ distribution from 175 to 177 Å for the 31-bp C2 substrate and negligibly for the 71-bp C2 substrate (Figs. 2 *A* and *C* and 3 and Table 1). In contrast, ATP addition to M2/MutS complex caused substantial changes (Figs. 2 *B* and *D* and 3 and Table 1). For the 31-bp M2 substrate, ATP shifted the peak in the $P(D_{i,j})$ distribution from 159 to 176 Å, which was almost the distance observed for the unbound substrate. A small subpopulation at the 110 Å contact distance was persistent. Addition of ATP to the 71-bp M2/MutS complex shifted the distance from 265 to 296 Å (Fig. 3*D*), indicating that ATP eliminated the MutS-induced bend. Retention of MutS on the gold-labeled DNA was confirmed by EMSA (*SI Appendix*, Fig. S7). Interestingly, in the presence of both MutS and ATP, the measured distance for 71-bp C2 was 7 Å longer than for free DNA, which suggests a decrease in DNA flexibility caused by loading multiple MutS homodimers, as also seen in surface plasmon resonance experiments (21, 22). Together, these data indicate that under conditions that generate the sliding clamps of MutS, DNA was not substantially bent.

Table 1. DNA end-to-end distributions

Condition	Peak max (Å)	Half-max Low (Å)	Half-max High (Å)	Mean Peak Position (Å)
31 C2	182	157	207	181
31 C2 S	175	151	199	171
31 C2 S ATP	177	149	203	173
31 M2	181	155	207	179
31 M2 S	159	110	186	150
31 M2 S ATP	176	146	201	168
31 M2 S L	159	108	184	149
31 M2 S L ATP	184	161	207	180
61 C2	269	235	302	258
71 C2	287	261	313	285
71 C2 S	286	260	312	284
71 C2 S ATP	287	264	310	286
71 M2	289	265	309	284
71 M2 S	265	227	289	251
71 M2 S ATP	296	278	314	296
71 M2 S L	254	208	289	242
71 M2 S L ATP	300	280	319	298

Max, Maximum; L, MutL; S, MutS;

MutL Does Not Trap Bent Conformations of DNA. MutS bound to mispair-containing DNA recruits MutL under conditions similar to sliding clamp formation, and this recruitment is required for MMR progression. We therefore investigated the effects of MutS and MutL on the DNA conformation by adding equivalent and excess amounts of MutL to preformed M2/MutS complexes in the absence or presence of ATP. MutL previously had been shown to bind to DNA/MutS complexes where the DNA was as short as 46 or 60 bp but not as short as 37 or 42 bp (39–41); thus, we investigated both 31- and 71-bp substrates. In the absence of ATP, where MutL is not expected to bind M2/MutS complexes, the $P(D_{i,j})$ distributions are similar to the M2/MutS complex alone for both the 31- and 71-bp substrates (Fig. 4 *A* and *B*). Upon adding 100-fold excess ATP relative to MutS, the peak of the $P(D_{i,j})$ distribution shifted to distances 3 and 11 Å longer than unbound DNA for both 31- and 71-bp substrates, respectively (Table 1). These distances were slightly longer than the distances measured under conditions under which MutS forms sliding clamps. In the case of the 71-bp substrate, we observed that 25% of the $P(D_{i,j})$ distribution did not shift upon addition of ATP. Given that MutL has a tendency to aggregate, this component of the shorter distribution might be due to a MutL-mediated association between multiple DNA substrates. We tested this by adding combinations of MutS, MutL, and ATP to a 71-bp singly labeled DNA with a central mismatch (M1). CSFs for the 71-bp M1 only had features in the presence of MutL (Fig. 4*C*), revealing that the short distance correlations were between nanocrystals on different DNAs rather than between nanocrystals on the same DNA. Thus, these data indicate that MutL recruitment does not stabilize MutS-induced bends on DNA but can lead to a MutL-mediated association between multiple DNAs on the 71-bp substrate consistent with the fact that the 71-bp substrate is long enough to support an interaction between MutL and MutS.

Discussion

Despite the available crystal structures of MutS and MutS homologs bound to mispair-containing DNAs (2, 4, 18, 30), biochemical and genetic evidence suggests that crucial aspects of the function of MutS involve conformational states that have yet to be characterized at an atomic level (21, 22, 24, 42, 43). Here, we demonstrate the compatibility of PEG-coated gold labels on DNA with proteins and follow the effects of MutS conformational states and MutS/MutL association on DNA conformations. For these studies, the increase in scattering power of the gold nanocrystals robustly enabled challenging measurements that involved low protein concentrations, long but biologically relevant distances, and buffer conditions optimized for MutS binding to DNA. Additionally, the scattering power would also enable time-resolved SAXS studies with millisecond exposures. This gold nanocrystal technique provided insights into MMR initiation and shows potential to analyze DNA conformations in transcription, replication, and repair processes that would be otherwise difficult to characterize.

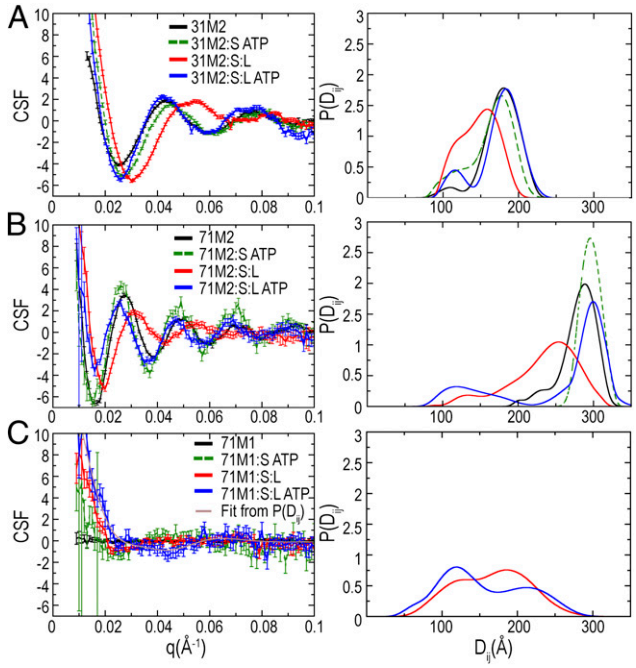

Fig. 4. MutL recruitment does not stabilize MutS-induced bends on DNA but can lead to a MutL-mediated association between DNAs based upon the CSF and $P(D_{i,j})$ distributions from doubly and singly labeled DNA in the presence of MutS, MutL, and ATP. (*A*) Doubly labeled 31-bp DNA with a single centrally located G/T mismatch. (*B*) Doubly labeled 71-bp DNA with a single centrally located G/T mismatch. (*C*) Singly labeled 71-bp DNA with a single centrally located G/T mismatch. Shown are DNA substrates alone (black) in the presence of MutS and ATP (green dashes), MutS and MutL (red), and MutS MutL and ATP (blue). The fit of the $P(D_{i,j})$ distribution from the singly labeled 71-bp DNA with MutS, MutL, and ATP is shown (*C*, gray).

In the absence of nucleotide or when bound to ADP, MutS recognizes and stably binds mispair-containing DNAs with ∼10 to 20-fold increased relative affinity to csDNA (44, 45). Our SAXS data indicated that MutS binds and bends mispair-containing DNAs from linear by ∼50–60°, supporting and extending data from crystal structures (2, 4, 18, 30). In contrast, the reduction of distances was far smaller for csDNAs. Observations of MutS bending of csDNA by atomic force microscopy (AFM) have been used to argue that bending is equivalent for both csDNA and mismatch-containing DNA (46). Binding of MutS along the entire length of a complementary substrate would reduce the observed bend angle and would be consistent with the smaller effect of MutS binding on the 71-bp C2 substrate than on the 31-bp C2 substrate; however, the estimated bend predicted by this model is still larger than the bend angles observed here. Thus, our data indicate that the equilibrium bending of csDNA is less than that of mispair-containing DNA and suggest that interactions with a solid surface in AFM might stabilize transient MutS/DNA conformations.

Challenging mispair-bound MutS with ATP induces a conformational change into a sliding clamp that readily moves along DNA but becomes trapped on DNAs with blocked ends (21, 22, 39, 42). The measured $P(D_{i,j})$ distributions for these samples show that the MutS-induced bend observed on mispair-containing DNAs was lost, indicating that the sliding clamp involves a conformational change that eliminates the interaction of the mispair with the mispair-binding domain. This mispair release explains the increased accessibility of these residues in deuterium exchange experiments (24) and the rapid motion of Msh2–Msh6 in single-molecule optical microscopy (31, 32). Surprisingly, the 71-bp M2 substrate had measured label-to-label distances that were 7 Å longer than the unbound M2 substrate, whereas a similar increase was not observed with the 31-bp M2 substrate. The loading of multiple MutS homodimers or MutS homologs under conditions under which sliding clamps can be formed has been experimentally observed (21, 22, 42). By combining an atomic model of the DNA/MutS complex (2) with our $P(D_{ij})$ distributions, the change in the flexible bent form to the more rigid form adopted in the presence of ATP is shown in Fig. 5. The reduction of DNA flexibility by the binding of multiple MutS homodimers explains the increase in label-to-label distances with the 71-bp M2 substrate and the lack of increase with the 31-bp M2 substrate, as this substrate is too short to bind multiple MutS homodimers.

An unobstructed DNA helix is critical for subsequent steps in MMR (26); yet, sliding clamp formation could be an abortive MutS reaction in the absence of MutL. MutL homologs have been reported to increase the affinity and residence time of MutS homologs to heteroduplex DNA (39, 47), and a proposed mechanism for MutL recognition of MutS involves stabilization of a MutS-bent mispair containing DNA rather than protein movement along the DNA (15). Our SAXS results provided no evidence that MutL binding involves stabilization of a bent form of the DNA substrate. Our data, which indicate that DNA bending only acts in initial mispair recognition, support models in which MutL or MutS/MutL complexes migrate along unbent DNA after MutS recognizes a mispair and binds ATP (21, 22, 48, 49). The eukaryotic system is likely similar, given that mutant Msh2 and Msh6 proteins, whose only clear biochemical defect is an inability to form sliding clamps, cause in vivo MMR defects (50).

Combining gold nanocrystals and SAXS has key advantages generally applicable to DNA/protein interactions. Label size can be adjusted to match the desired time scale or concentration regimes in solution. Probed length scales exceed distances measurable by fluorescence resonance energy transfer (51) or spin coupling (52). Importantly for DNA/protein interactions, SAXS with gold nanocrystals provides information on the distribution of distances and not just the average distance, allowing visualization of ensembles and identification of potential substoichiometric fractions (like those observed for MutL; Fig. 4*B*) of a population possessing different interlabel distances. Conformational changes of DNA, mediated by complex cascades, as observed here in MMR, are likely properties of DNA transcription, replication, recombination, and repair. We therefore anticipate related strategies will aid studying these and other complex systems, which cannot be robustly examined by classical techniques. Looking forward, examining DNA with gold labels as single molecules or in fluctuation scattering experiments from a few molecules enabled by next-generation light sources with fluxes many orders of magnitudes brighter has significant potential.

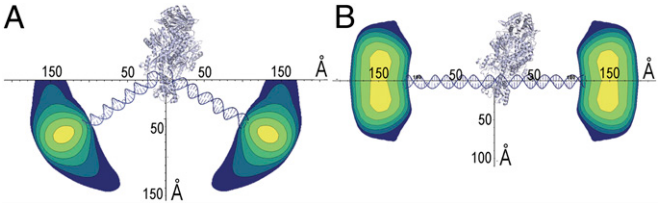

Fig. 5. Mismatch DNA bending by MutS and straightening in the presence of ATP. Contour plots of the distribution of DNA ends are visualized by placing the structural information from the crystal structure of MutS/DNA (2) on the same scale as the distance and population information from the *P(Dij)* distributions. The $P(D_{ij})$ distributions from 71-bp DNA in the presence of MutS (*A*) and the presence of MutS and excess ATP (*B*) set contour levels. The widest part of the distribution is the width of the gold nanocrystal. DNA of the crystal structure has been extended to 71 bp for the MutS/DNA complex and replaced by straight DNA for the ATP model.

Methods

Synthesis and Purification of DNA with Gold Nanocrystal Labels. Details of the generation of the gold nanocrystal labels are provided in *SI Appendix, SI Methods*. Briefly, citrate-conjugated gold nanocrystals were converted to bis-(*p*-sulfonatophenyl) phenylphosphine-liganded nanocrystals. These were then conjugated to DNA oligonucleotides with 5′ monothiol or 5′ trithiol modifications. A neutral thiolated PEG ligand was then liganded to the gold, and the products were purified. Purified products were then annealed to generate labeled dsDNA substrates.

Expression and Purification of *E. coli* MutS and MutL. His6-MutS and His6-MutL were overexpressed in BL21 cells containing plasmids pTX412 and pTX418 (gifts of Malcom Winkler, Indiana University), respectively, and were purified as described previously (36, 53). Briefly, the His-tagged proteins were purified over a nickel column followed by a Mono-Q column. Proteins aliquots were frozen in liquid nitrogen and stored at −80 °C.

SAXS Data Collection and Processing. Details of the SAXS data collection and processing to extract interlabel distance information are provided in *SI Appendix, SI Methods*. Briefly, all SAXS experiments were collected at the SIBYLS beamline (beamline 12.3.1) at the Advanced Light Source at Lawrence Berkeley National Laboratory, with an X-ray energy of 8 keV (54). The CSF was derived from the experimental scattering profile by fitting of the gold label scattering $G(q)$, by an ellipsoid of revolution in the low q region, and by fitting a constant to ensure that the CSF oscillated about zero. The CSF was then transformed using the GIFT method (28) to derive $P(D_{i,j})$ distributions.

ACKNOWLEDGMENTS. This work was supported by National Institutes of Health (NIH) Structural Cell Biology of DNA Repair Machines Grant P01 CA092584 (to J.A.T. and R.D.K.), by NIH Grant GM50006 (to R.D.K.), and by the Berkeley Laboratory Directed Research and Development funds provided by the Director, Office of Science, US Department of Energy (DOE). The SIBLYS beamline efforts were supported by the DOE Integrated Diffraction Analysis Technologies program and NIH Grant GM105404. The DOE Office of Science, Basic Energy Sciences, Contract DE-AC02-05CH11231, supported A.P.A.'s contribution.

1. Dinner AR, Blackburn GM, Karplus M (2001) Uracil-DNA glycosylase acts by substrate autocatalysis. *Nature* 413(6857):752–755.
2. Lamers MH, et al. (2000) The crystal structure of DNA mismatch repair protein MutS binding to a G x T mismatch. *Nature* 407(6805):711–717.
3. Min JH, Pavletich NP (2007) Recognition of DNA damage by the Rad4 nucleotide excision repair protein. *Nature* 449(7162):570–575.
4. Obmolova G, Ban C, Hsieh P, Yang W (2000) Crystal structures of mismatch repair protein MutS and its complex with a substrate DNA. *Nature* 407(6805):703–710.
5. Tsutakawa SE, et al. (2011) Human flap endonuclease structures, DNA double-base flipping, and a unified understanding of the FEN1 superfamily. *Cell* 145(2):198–211.
6. Williams RS, et al. (2008) Mre11 dimers coordinate DNA end bridging and nuclease processing in double-strand-break repair. *Cell* 135(1):97–109.
7. Vainshtein BK, et al. (1980) Determination of the distance between heavy-atom markers in haemoglobin and histidine decarboxylase in solution by small-angle x-ray scattering. *FEBS Lett* 116(1):107–110.
8. Miake-Lye RC, Doniach S, Hodgson KO (1983) Anomalous x-ray scattering from terbium-labeled parvalbumin in solution. *Biophys J* 41(3):287–292.
9. Mathew-Fenn RS, Das R, Harbury PA (2008) Remeasuring the double helix. *Science* 322(5900):446–449.
10. Mathew-Fenn RS, Das R, Silverman JA, Walker PA, Harbury PA (2008) A molecular ruler for measuring quantitative distance distributions. *PLoS ONE* 3(10):e3229.
11. Mastroianni AJ, Sivak DA, Geissler PL, Alivisatos AP (2009) Probing the conformational distributions of subpersistence length DNA. *Biophys J* 97(5):1408–1417.
12. Hura GL, et al. (2013) Comprehensive macromolecular conformations mapped by quantitative SAXS analyses. *Nat Methods* 10(6):453–454.
13. Hura GL, et al. (2009) Robust, high-throughput solution structural analyses by small angle X-ray scattering (SAXS). *Nat Methods* 6(8):606–612.
14. Putnam CD, Hammel M, Hura GL, Tainer JA (2007) X-ray solution scattering (SAXS) combined with crystallography and computation: defining accurate macromolecular structures, conformations and assemblies in solution. *Q Rev Biophys* 40(3):191–285.
15. Kunkel TA, Erie DA (2005) DNA mismatch repair. *Annu Rev Biochem* 74:681–710.
16. Modrich P, Lahue R (1996) Mismatch repair in replication fidelity, genetic recombination, and cancer biology. *Annu Rev Biochem* 65:101–133.
17. Li GM (2008) Mechanisms and functions of DNA mismatch repair. *Cell Res* 18(1):85–98.
18. Warren JJ, et al. (2007) Structure of the human MutSalpha DNA lesion recognition complex. *Mol Cell* 26(4):579–592.
19. Iyer RR, Pluciennik A, Burdett V, Modrich PL (2006) DNA mismatch repair: functions and mechanisms. *Chem Rev* 106(2):302–323.
20. Blackwell LJ, Wang S, Modrich P (2001) DNA chain length dependence of formation and dynamics of hMutSalpha.hMutLalpha.heteroduplex complexes. *J Biol Chem* 276(35):33233–33240.
21. Mendillo ML, Mazur DJ, Kolodner RD (2005) Analysis of the interaction between the Saccharomyces cerevisiae MSH2-MSH6 and MLH1-PMS1 complexes with DNA using a reversible DNA end-blocking system. *J Biol Chem* 280(23):22245–22257.
22. Acharya S, Foster PL, Brooks P, Fishel R (2003) The coordinated functions of the E. coli MutS and MutL proteins in mismatch repair. *Mol Cell* 12(1):233–246.
23. Mendillo ML, et al. (2009) A conserved MutS homolog connector domain interface interacts with MutL homologs. *Proc Natl Acad Sci USA* 106(52):22223–22228.
24. Mendillo ML, et al. (2010) Probing DNA- and ATP-mediated conformational changes in the MutS family of mispair recognition proteins using deuterium exchange mass spectrometry. *J Biol Chem* 285(17):13170–13182.
25. Owen BAL, Lang WH, McMurray CT (2009) The nucleotide binding dynamics of human MSH2-MSH3 are lesion dependent. *Nat Struct Mol Biol* 16(8):897–897.
26. Pluciennik A, Modrich P (2007) Protein roadblocks and helix discontinuities are barriers to the initiation of mismatch repair. *Proc Natl Acad Sci USA* 104(31):12709–12713.
27. Warren BE (1990) *X-Ray Diffraction* (Dover, New York).
28. Glatter O (1977) New method for evaluation of small-angle scattering data. *J Appl Crystallogr* 10(5):415–421.
29. Olson WK, Gorin AA, Lu XJ, Hock LM, Zhurkin VB (1998) DNA sequence-dependent deformability deduced from protein-DNA crystal complexes. *Proc Natl Acad Sci USA* 95(19):11163–11168.
30. Gupta S, Gellert M, Yang W (2012) Mechanism of mismatch recognition revealed by human MutSβ bound to unpaired DNA loops. *Nat Struct Mol Biol* 19(1):72–78.
31. Gorman J, et al. (2007) Dynamic basis for one-dimensional DNA scanning by the mismatch repair complex Msh2-Msh6. *Mol Cell* 28(3):359–370.
32. Jeong C, et al. (2011) MutS switches between two fundamentally distinct clamps during mismatch repair. *Nat Struct Mol Biol* 18(3):379–385.
33. Cho WK, et al. (2012) ATP alters the diffusion mechanics of MutS on mismatched DNA. *Structure* 20(7):1264–1274.
34. Lamers MH, et al. (2004) ATP increases the affinity between MutS ATPase domains. Implications for ATP hydrolysis and conformational changes. *J Biol Chem* 279(42): 43879–43885.
35. Bjornson KP, et al. (2003) Assembly and molecular activities of the MutS tetramer. *J Biol Chem* 278(36):34667–34673.
36. Mendillo ML, Putnam CD, Kolodner RD (2007) Escherichia coli MutS tetramerization domain structure reveals that stable dimers but not tetramers are essential for DNA mismatch repair in vivo. *J Biol Chem* 282(22):16345–16354.
37. Manelyte L, Urbanke C, Giron-Monzon L, Friedhoff P (2006) Structural and functional analysis of the MutS C-terminal tetramerization domain. *Nucleic Acids Res* 34(18): 5270–5279.
38. Sass LE, Lanyi C, Weninger K, Erie DA (2010) Single-molecule FRET TACKLE reveals highly dynamic mismatched DNA-MutS complexes. *Biochemistry* 49(14):3174–3190.
39. Schofield MJ, Nayak S, Scott TH, Du CW, Hsieh P (2001) Interaction of Escherichia coli MutS and MutL at a DNA mismatch. *J Biol Chem* 276(30):28291–28299.
40. Sedletska Y, Culard F, Midoux P, Malinge JM (2013) Interaction studies of muts and mutl with DNA containing the major cisplatin lesion and its mismatched counterpart under equilibrium and nonequilibrium conditions. *Biopolymers* 99(9):636–647.
41. Winkler I, et al. (2011) Chemical trapping of the dynamic MutS-MutL complex formed in DNA mismatch repair in Escherichia coli. *J Biol Chem* 286(19):17326–17337.
42. Gradia S, et al. (1999) hMSH2-hMSH6 forms a hydrolysis-independent sliding clamp on mismatched DNA. *Mol Cell* 3(2):255–261.
43. Qiu RY, et al. (2012) Large conformational changes in MutS during DNA scanning, mismatch recognition and repair signalling. *EMBO J* 31(11):2528–2540.
44. Fishel R (1998) Mismatch repair, molecular switches, and signal transduction. *Genes Dev* 12(14):2096–2101.
45. Kolodner R (1996) Biochemistry and genetics of eukaryotic mismatch repair. *Genes Dev* 10(12):1433–1442.
46. Wang H, et al. (2003) DNA bending and unbending by MutS govern mismatch recognition and specificity. *Proc Natl Acad Sci USA* 100(25):14822–14827.
47. Habraken Y, Sung P, Prakash L, Prakash S (1997) Enhancement of MSH2-MSH3-mediated mismatch recognition by the yeast MLH1-PMS1 complex. *Curr Biol* 7(10):790–793.
48. Elez M, Radman M, Matic I (2012) Stoichiometry of MutS and MutL at unrepaired mismatches in vivo suggests a mechanism of repair. *Nucleic Acids Res* 40(9):3929–3938.
49. Hombauer H, Campbell CS, Smith CE, Desai A, Kolodner RD (2011) Visualization of eukaryotic DNA mismatch repair reveals distinct recognition and repair intermediates. *Cell* 147(5):1040–1053.
50. Hargreaves VV, Shell SS, Mazur DJ, Hess MT, Kolodner RD (2010) Interaction between the Msh2 and Msh6 nucleotide-binding sites in the Saccharomyces cerevisiae Msh2-Msh6 complex. *J Biol Chem* 285(12):9301–9310.
51. Hohlbein J, Gryte K, Heilemann M, Kapanidis AN (2010) Surfing on a new wave of single-molecule fluorescence methods. *Phys Biol* 7(3):031001.
52. Schiemann O, et al. (2004) A PELDOR-based nanometer distance ruler for oligonucleotides. *J Am Chem Soc* 126(18):5722–5729.
53. Feng G, Winkler ME (1995) Single-step purifications of His6-MutH, His6-MutL and His6-MutS repair proteins of escherichia coli K-12. *Biotechniques* 19(6):956–965.
54. Classen S, et al. (2013) Implementation and performance of SIBYLS: A dual endstation small-angle X-ray scattering and macromolecular crystallography beamline at the Advanced Light Source. *J Appl Cryst* 46(Pt 1):1–13.